Fusion of local normalization and Gabor entropy weighted features for face identification

Leonardo A. Cament *, Luis E. Castillo, Juan P. Perez, Francisco J. Galdames, Claudio A. Perez

Image Processing Laboratory, Department of Electrical Engineering and Advanced Mining Technology Center, Universidad de Chile, Av. Tupper 2007, Santiago, Chile

ABSTRACT

Face recognition is one of the most extensively studied topics in image analysis because of its wide range of possible applications such as in surveillance, access control, content-based video search, human–computer interaction, electronic advertisement and more. Face identification is a one-to-n matching problem where a captured face is compared to n samples in a database. In this work we propose two new methods for face identification. The first one combines entropy-like weighted Gabor features with the local normalization of Gabor features. The second fuses the entropy-like weighted Gabor features at the score level with the local binary pattern (LBP) applied to the magnitude (LGBP) and phase (LGXP) components of the Gabor features. We used the FERET, AR, and FRGC 2.0 databases to test and compare our results with those previously published. Results on these databases show significant improvement relative to previously published results, reaching the best performance on the FERET and AR databases. Our methods also showed significant robustness to slight pose variations. We tested the proposed methods assuming noisy eye detection to check their robustness to inexact face alignment. Results show that the proposed methods are robust to errors of up to 3 pixels in eye detection.

© 2013 Elsevier Ltd. All rights reserved.

1. Introduction

Face identification is a one-to-n matching problem where the goal is to identify a person based on the face image, i.e., the captured face needs to be compared to n samples in the database [1]. Typical applications for face identification are used in immigration, access control, and law enforcement, agencies that try to answer the question, "Who is this person?". Face recognition is one of the most popularly studied topics in image analysis because of its wide range of possible applications, such as in surveillance, access control, information security, content-based video search, human–computer interfaces, electronic marketing and advertising, and entertainment [2]. In spite of more than 20 years of intense research in face recognition, many real world situations are still a challenge. Uncontrolled conditions such as illumination changes, varying gestures, pose, and occlusions still present unsolved problems [3].

Some approaches to face recognition have focused on face and eye localization in which faces are cropped and aligned, which could be a crucial step [4–7]. An appreciable number of papers have

focused directly on face recognition on the assumption that the face has already been localized [8,9]. We center our literature review on the methods that have been used the most and have yielded the highest face recognition performance on available face databases.

Holistic approaches use the image as vector data and in some cases they reduce the data dimension by feature selection and by frequency component discrimination. Among the most widely used methods for face recognition based on feature extraction are eigenfaces [10], a holistic method that uses Principal Component Analysis (PCA) to project the image data vector into a reduced space, maximizing the variance of the data; and Fisherfaces [11], which is based on Linear Discriminant Analysis (LDA), maximizes the distance between classes and minimizes the distance between prototypes within each class; and methods based on Independent Component Analysis (ICA) [12,13]. Other methods for face recognition are based on frequency space as a discrete cosine transform (DCT) [14,15], that compares DCT–based feature vectors from different images, and the Walsh–Hadamard transform (WHT) [16], a low complexity algorithm that compares WHT-based feature vectors.

There are also methods that use a linear combination of training images to reconstruct the testing image, such as Sparse representation-based methods (SRC) [17]. In [18], SRC was used to align faces with variations of pose reaching good results on the Multi-PIE database [19]. This method is more robust to occlusions, noise, illumination changes, and varying pose compared with other previously

---

* Corresponding author. Tel.: +56 2 678 4196; fax: +56 2 695 3881.

E-mail addresses: lcament@ing.uchile.cl (L.A. Cament), luiscast@ing.uchile.cl (L.E. Castillo), juanpper@ing.uchile.cl (J.P. Perez), fgaldame@ing.uchile.cl (F.J. Galdames), clperez@ing.uchile.cl (C.A. Perez).

published methods. Another important aspect of this method is that no information is lost as in those based on feature extraction. Nevertheless, this method [17,18] requires several enrolled images with different poses which may not be available in practical applications. A sparse correntropy method which shows more robustness and efficiency with recognition of occluded and corrupted face images is proposed in [20].

Recently, local feature-based methods for face recognition have shown improved robustness to changes in illumination, gesticulation and occlusion. The local binary pattern (LBP) method was proposed in [21] where the face image is divided into square windows and a binary 1 is generated in the code whenever a pixel exceeds the value of the central pixel; otherwise a 0 is generated into the code.

Gabor wavelets [22–25] have been used to extract local features achieving outstanding results in face recognition. Among the methods based on Gabor Wavelets are the Elastic Bunch Graph Matching (EBGM) method [26], Gabor Fisher Classifier (GFC) [27], Local Gabor Binary Pattern Histogram Sequence (LGBPHS) [28], Histogram of Gabor Phase Patterns (HGPP) [29], Local Gabor Textons (LGT) [30], Learned Local Gabor Pattern (LLGP) [31], Local Gabor Binary Pattern Whitening PCA (LGBPWP) [32], and Local Matching Gabor method (LMG) [33]. In the LMG method each Gabor feature is considered as an independent classifier that is combined using the Borda count method [33,34].

In [35–37], improvements on the LMG method were reported, performed by weighting Gabor jets by an entropy measure between a given face and the faces in the gallery. Another improvement was carried out in the combination of the classifiers stage where a threshold was introduced to eliminate low jet comparison values that acted like noisy inputs. The local normalization (LN) illumination compensation method [37] used with the LMG showed significant improvements. The LMG method was also improved as shown in [36] by using a weighted strategy with entropy. An alternative way of using Gabor features was proposed in [38], in which a 3D image model was enrolled, and for recognition, a 2D model was built and matched with the 3D model.

In [39] the face was divided into patches without overlap, and then the best patches were selected and weighted with an LDA strategy in a greedy search. Finally, the local scores of the patches were combined with a global score obtained from the low frequency components of the FFT applied to the whole face including its external boundary. In [40] magnitude and phase Gabor features were combined using the LBP operator. This method, using a greedy search and the FERET and FRGC 2.0 databases, obtained the best result in face recognition published to date. The details about this method are given in Section 2.2.

In this work, we propose a new method, LMGEW//LN, which is the result of an entropy-like weighted strategy for the LMG method, combined with the LN image. We also propose another method which consists of fusing the LMGEW//LN method at the score level with the LGBP and LGXP methods, the latter proposed in [40]. We used the FERET, AR, and FRGC 2.0 databases to test and compare our results with the previously published FERET and FRGC 2.0 defined standard experiments [41–43]. In these experiments, all images in each different subset are fixed. In this form, the same conditions are set to compare different methods. Our proposed method is designed to improve face identification by taking advantage of the comparison performed against all gallery images.

2. Related work

2.1. Gabor wavelet

The Gabor kernel is given by $\Psi_{\mu,\nu}$. In (1), z represents the pixel coordinate, μ is the orientation, ν is the scale, f is the step in

frequency, and k_{max} is the maximum frequency. In this work we use five scales ($0 \leq \nu \leq 4$) and eight orientations ($0 \leq \mu \leq 7$) for the Gabor filters as in [33,39,40]

$$\Psi_{\mu,\nu}(\vec{z}) = \frac{|\vec{k}|^2}{\sigma^2}\exp\left(-\frac{|\vec{k}|^2|\vec{z}|^2}{2\sigma^2}\right)\left[\exp(i\vec{k}\cdot\vec{z})-\exp\left(-\frac{\sigma^2}{2}\right)\right]$$

$$\vec{z} = (x,y)^T, \quad \vec{k} = \frac{k_{max}}{f^\nu}\left[\cos\left(\pi\frac{\mu}{8}\right), \sin\left(\pi\frac{\mu}{8}\right)\right]^T \tag{1}$$

A Gabor feature is obtained by finding the convolution between the image $I(\vec{z})$ and the kernel $\Psi_{\mu,\nu}(\vec{z})$, i.e. $G_{\mu,\nu}(\vec{z}) = I(\vec{z})*\Psi_{\mu,\nu}(\vec{z})$. The Gabor feature has both a real and an imaginary part, and in this work we use the magnitude and phase features separately. Magnitude $M_{\mu,\nu}(\vec{z})$ and phase $P_{\mu,\nu}(\vec{z})$ are computed by (2) and (3)

$$M_{\mu,\nu}(\vec{z}) = \sqrt{Im(G_{\mu,\nu}(\vec{z}))^2 + Re(G_{\mu,\nu}(\vec{z}))^2} \tag{2}$$

$$P_{\mu,\nu}(\vec{z}) = \arctan\left(\frac{Im(G_{\mu,\nu}(\vec{z}))}{Re(G_{\mu,\nu}(\vec{z}))}\right) \tag{3}$$

2.2. Review of LGBP and LGXP

The method proposed in [40] combines local binary pattern (LBP) applied to the magnitude component of the Gabor features (LGBP), and the local XOR operator (LXP) applied to the phase component of the Gabor features (LGXP) for face recognition. As shown in Fig. 1 the method consists of the extraction of LGBP and LGXP [40] features from the image. The image is divided into blocks and each block into sub-blocks. For every sub-block a histogram is computed and for each block the sub-block histograms are concatenated. Then LDA is applied to reduce the histogram dimensionality, selecting the most significant features. LGBP and LGXP are combined at the score or feature level using $S = w \cdot S_{LGBP} + (1-w) \cdot S_{LGXP}$, where S_{LGBP} is the LGBP score, S_{LGXP} is the LGXP score, and w is the weight relation between LGBP and LGXP features.

2.3. Review of LMG

The LMG method [33,35] uses magnitude Gabor features taken at fixed locations within five different grids for five spatial frequencies as shown in Fig. 2. It has been shown that fixing locations for feature extraction is a good strategy because magnitude features are robust to small spatial variations [33]. The features extracted by the Gabor kernel for the five spatial frequencies $\nu = \{0, 1, 2, 3, 4\}$ are separated at distances given by their wavelength $\lambda = \{4, 4\sqrt{2}, 8, 8\sqrt{2}, 16\}$.
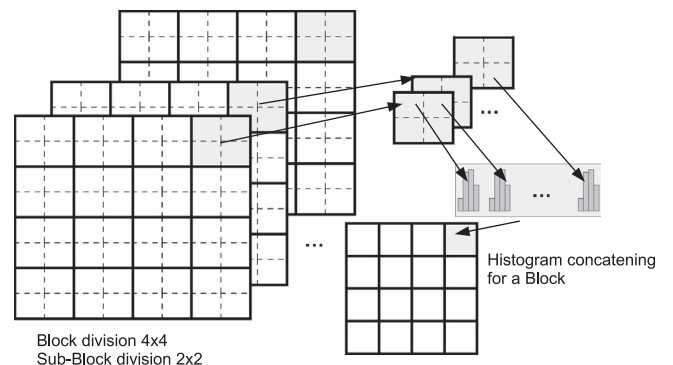

Block division 4x4
Sub-Block division 2x2

Histogram concatening
for a Block

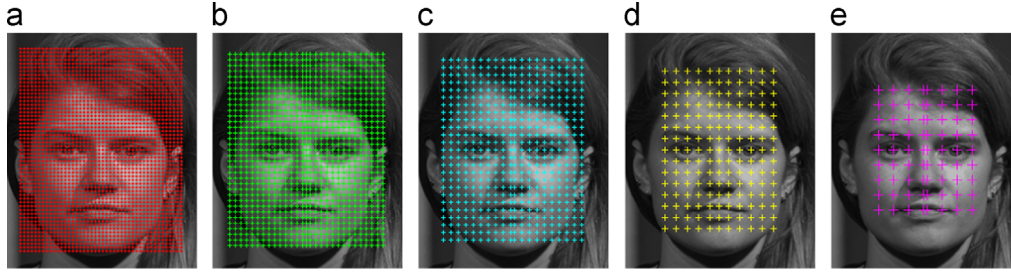**Fig. 1.** Division of blocks and sub-blocks of LGBP.

Fig. 2. A face from the FERET database with the five grids for spatial scales (a) $\nu = 0$, (b) $\nu = 1$, (c) $\nu = 2$, (d) $\nu = 3$ and (e) $\nu = 4$. The + sign represents the spatial point on the grid where the Gabor jet is computed.

The images are rotated, displaced and resized so that the eyes are located in a fixed position. The new eye positions are $(67, 125)$ and $(135, 125)$ in a 203×251 size image. The grids are defined by the wavelength λ of the Gabor jets, in the same way as they were described in [33,35].

Magnitude Gabor features are extracted in the locations shown by the five grids in Fig. 2, using the Gabor kernel in (1) of eight orientations and five spatial scales. Each spatial scale corresponds to one of the five grids. The fixed parameters are $k_{max} = \pi/2$ and $f = \sqrt{2}$. In each coordinate of the five grids, eight Gabor features are computed corresponding to the eight orientations. These eight values are concatenated in a vector that is called a *jet*. Therefore, five sets of jets corresponding to different scales are computed for each image, making a total of N jets. The spatial information is preserved implicitly because the image was transformed to locate the eyes in a fixed position and the jets are computed in the same positions in every image. The jet computation is the same as was previously used in [33,35].

The jets of target image are compared with the N jets of the M gallery images in the database, creating an $M \times N$ comparison matrix C. The comparison of a pair of jets is performed by cosine distance $C_{i,j} = J_j^T \cdot J_{i,j}^G / (\| J_j^T \| \cdot \| J_{i,j}^G \|)$, where J_j^T is the jth jet of the test image, and $J_{i,j}^G$ is the jth jet of the ith gallery image.

Each jet is considered as an independent classifier that is combined using the voting method Borda count [34,44]. Borda count is applied on all vectors formed with every column of matrix C. The Borda count consists of ranking the comparison values, assigning 0 to the lowest value, 1 to the second lowest value, up to $M - 1$ for the highest value. This ranking matrix is denoted as O, and in the Borda count, the score of each candidate is given by the sum of rankings of all classifiers, $B_i = \sum_{j=1}^{N} O_{i,j}$.

3. Local matching Gabor entropy-like weighted with LN features (LMGEW//LN-BTH)

There are two parallel stages in fusing LMGEW and LN. The first stage computes the entropy-like weighted vector (Fig. 3(a)). The second stage computes the Borda count from the LN input image I_{LN} (Fig. 3(b)). A Borda count threshold (BTH) is used to eliminate from Gabor jet comparison matrix with low values that act as noise in the identification procedure. A block diagram of LMGEW// LN-BTH is shown in Fig. 3.

3.1. Entropy-like weighted vector

The proposed entropy-like measure estimates the variability of the similarity of the Gabor feature in the position (x, y, λ) of the target image with respect to the same feature in the whole gallery set. Each Gabor feature is represented by a jet. Entropy has its maximum value when probabilities of different states are the
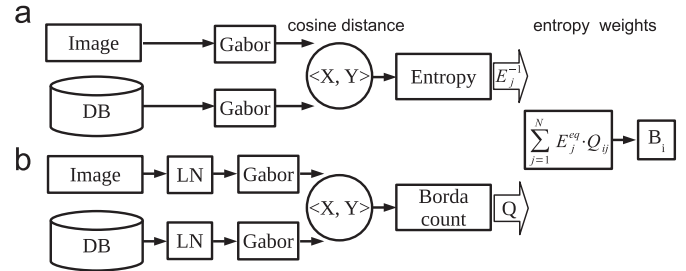

Fig. 3. Block diagram of LMGEW//LN-BTH. (a) Computation of the entropy-like weighted vector. (b) Computation of the Borda count using LN.

same, and lower values when probabilities are different. The states are the comparison values between jets from the target image and the gallery set. Therefore, entropy provides quantitative information to determine if a jet can be used to distinguish faces in the database. Jets located in the face regions with low entropy should weight more in the final face recognition score. We estimated the probabilities using the histogram of the values resulting from the jets comparisons (C matrix). The values of C are quantized in K bins and the histogram for each jet along the database (rows of C) is computed. The values of the histograms are normalized by the number, M, of faces in the gallery, and are used as the probability $P_{j,k}$ that the comparison value $C_{i,j}$ of the jth jet is within the bin k.

The entropy-like value of the jth jet E_j is computed for each jet as shown in (4). Because jets with lower entropy-like value must be emphasized, the inverse of this value ($E_j^{-1} = 1/E_j$) is computed and normalized to the range [0,1]. Finally, E_j^{-1} is equalized to distribute the values uniformly, calling E^{eq} the equalized vector

$$E_j = - \sum_{k=1}^{K} P_{j,k} \cdot \log_2 P_{j,k} \qquad (4)$$

Fig. 4(a–e) shows an example of entropy weights, E^{eq}, computed for each spatial frequency. The example shows that features around the face, near the mouth and ears, have lower weights while features around the nose and eyes have higher weights, in this way indicating features that contribute most in the face identification process.

In order to visualize the entropy-like values we performed the following experiment. The average of each component of vector E^{eq} for the FERET training database was computed, and using a threshold, we selected those jets with 25% of the highest average E^{eq} where each spatial frequency was applied, as shown in Fig. 4(f–j). It can be observed that the most important selected features are located around the eyes and nose. At lower spatial scales, features around the mouth are also selected. At higher spatial scales the chin and the lower part of the cheeks are selected. It can also be seen that features on the forehead and external area around the face are not selected.
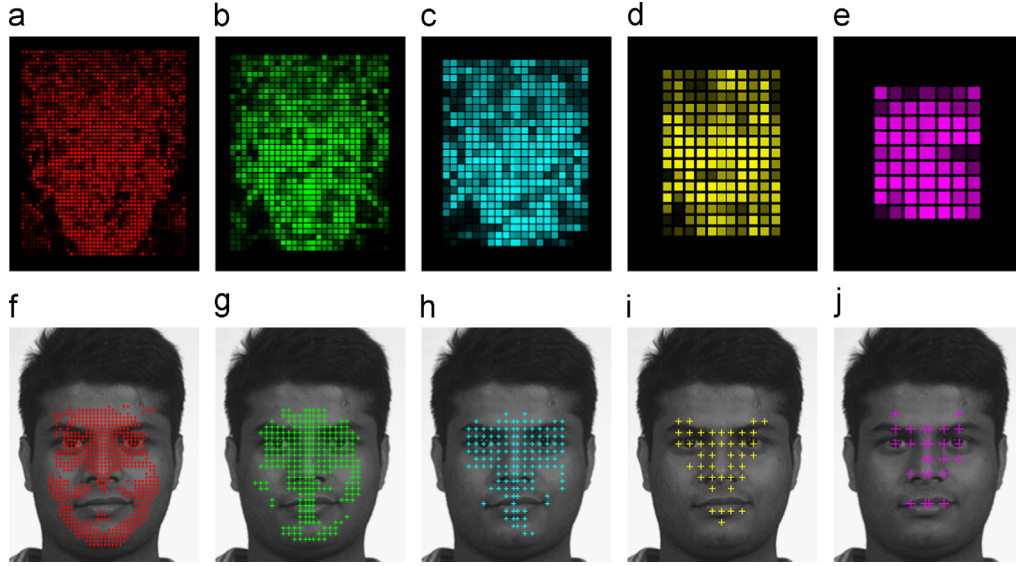
Fig. 4. (a–e) Computed equalized weights for jets at five spatial frequencies (a) $\nu = 0$, (b) $\nu = 1$, (c) $\nu = 2$, (d) $\nu = 3$ and (e) $\nu = 4$. The intensity color is proportional to the jet weight, i.e., a 0 weight is assigned to gray intensity 0, and a weight of 1 to the gray intensity 255. (f–j) Jets selected by the highest weight values (25%) for each spatial frequency: (f) $\nu = 0$, (g) $\nu = 1$, (h) $\nu = 2$, (i) $\nu = 3$ and (j) $\nu = 4$.

3.2. Borda count ranking matrix for LN images

In this stage, the image with local normalization features (LN) is used as the input image in the LMG method. In previous work [37] different methodologies for illumination compensation were combined and optimized, among them LN-LMG which improved significantly the LMG. As in the first step of Section 2.3, the image is rotated and resized to 203×251. Then, the LN image $I_{LN}(x,y)$ is given by (5), where $I_{mean}^{9 \times 9}(x,y)$ denotes the mean of a 9×9 neighborhood around the pixel (x,y), and $I_{std}^{9 \times 9}(x,y)$ is the standard deviation in the 9×9 neighborhood. Fig. 5(a) shows a face image and Fig. 5(b) shows the LN of the image

$$I_{LN}(x,y) = \frac{I(x,y) - I_{mean}^{9 \times 9}(x,y)}{I_{std}^{9 \times 9}(x,y) + 0.01} \qquad (5)$$

Gabor features of $I_{LN}(x,y)$ are computed using five scales and eight orientations, and a comparison matrix C_{LN} and ranking matrix O_{LN} are obtained [35]. A modified ranking matrix Q_{LN} is created by (6), where T_h is a threshold that eliminates noisy values. The BTH suffix is added to the method name when the matrix Q is used instead of O

$$Q_{i,j}^{LN} = \begin{cases} O_{i,j}, & C_{i,j} \geq T_h \\ 0, & C_{i,j} < T_h \end{cases} \qquad (6)$$

Finally, Q_{LN} is weighted with the entropy-like vector E^{eq}. An identification score $B_i = \sum_{j=1}^{N} E_j^{eq} \cdot Q_{i,j}^{LN}$ is obtained, and the highest score represents the person's identity.

3.3. Fusion of LMGEW//LN-BTH with LGBP and LGXP

Fusion of different methods is performed at the score level as follows. In the HEC algorithm [39] global features C_G are combined with local features C_L at the score level as $HEC = w \cdot C_G + (1-w) \cdot C_L$. In [40] LGBP and LGXP features are combined at the score level in the same way as HEC as shown in Section 2.2. We combine LMGEW//LN-BTH with LGBP and LGXP in the same way as in previous methods as shown in (7), where S_1 denotes the identification score of LMGEW//LN-BTH, and S_2 the score of LGBP
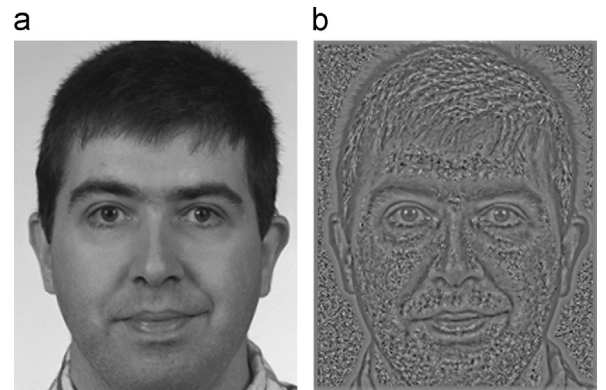

Fig. 5. (a) Original image and (b) local normalization image.

Table 1
A simulated example to illustrate the benefit of the fusion of two different methods. The scores are shown for two methods and their fusion for the comparison of one individual with him/herself (AA), with individual B (AB) or with individual C (AC).

Match	AA	AB	AC
Method 1	0.6	0.7	0.4
Method 2	0.6	0.3	0.7
Fusion	0.6	0.5	0.55

or LGXP, depending on which kind of feature is used

$$S = w \cdot S_1 + (1-w) \cdot S_2 \qquad (7)$$

The simulated example shown in Table 1 has matching scores for two methods (Methods 1 and 2) of three matches: AA (comparing two individuals of the same class match), AB (comparing one individual to another), and AC (comparing one individual to another). It can be observed that match AA is not the best for both methods, but nevertheless reaches the highest score in the fusion of both methods. This result can be explained when each different method (methods 1 and 2) uses different features to reach the score. Then both methods can combine the best features to reach the score for their fusion. In this case they will be combined synergistically

Table 2
Rank-1 face identification rate on different subsets of the FERET database for different face recognition methods published in the literature.

Methods	Accuracy (%)				Errors
	Fb	Fc	Dup1	Dup2	Total
LMG [33][a]	99.5	99.5	85.0	79.5	163
LGBPWP [32][a]	98.1	98.9	83.8	81.6	185
LLGP [31][a]	99.0	99.0	80.0	78.0	209
HGPP [29][a]	97.5	99.5	79.5	77.8	231
LGBPHS [28][a]	98.0	97.0	74.0	71.0	286
HEC [39][a]	99.00	99.00	92.00	88.00	99
LGBP+LGXP [40][a]	99.00	99.00	94.00	93.00	77
LMGEW [36]	99.75	**100.00**	87.40	85.47	128
LMGEW-BTH [36]	99.75	**100.00**	90.17	88.03	102
LMGEW//LN-BTH	99.83	**100.00**	92.66	89.74	79
LGBP[b]	99.08	98.45	85.60	77.35	171
LGXP[b]	97.66	96.39	79.64	75.64	239
LMGEW//LN+LGBP	**99.92**	**100.00**	**95.57**	**93.59**	**48**
LMGEW//LN+LGXP	**99.92**	**100.00**	94.74	91.88	58

[a] Results extracted from original source.
[b] Results obtained with our implementation of the method.

Table 3
Rank-1 face recognition rate for the AR database.

Gal S1 methods	Accuracy (%)			Errors
	S2-Normal	Scarves	Sunglasses	Total
LGBPHS [28][a]	–	98	80	–
SRC [17][a]	95.7	93.5	**97.5**	84
LMG-BTH [36]	99.00	98.83	89.50	77
LMGEW-BTH [36]	99.29	99.00	95.33	39
LMGEW//LN-BTH	99.29	98.83	95.00	45
LGBP	99.71	97.83	65.83	220
LGXP	97.86	94.33	73.67	213
LMGEW//LN+LGBP	**100.00**	**99.83**	95.50	29
LMGEW//LN+LGXP	**100.00**	99.67	96.33	**24**

[a] Results extracted from original source.

Table 4
Rank-1 face recognition rate on experiments 1 and 4 on the FRGC 2.0 database.

Methods	Accuracy (%)	
	Exp1	Exp4
LMG	99.08	86.15
LMG-BTH	99.23	89.10
LMGEW-BTH	99.62	89.71
LMGEW//LN-BTH	99.69	88.57

Table 5
Rank-1 face identification rate published in the literature and proposed methods on different subsets with varying pose of the FERET database.

Methods	Accuracy (%)				Errors
	bd	be	bf	bg	Total
LMG [35][a]	81.0	97.0	98.0	79.5	89
LMG-EJS-BIP-BTH [35][a]	93.5	98.5	98.0	91.5	37
LMGEW//LN-BTH	96.0	99.0	99.5	96.5	18
LGBP	86.5	98.0	97.5	88.5	60
LGXP	73.5	95.5	96.0	65.5	139
LMGEW//LN+LGBP	98.0	99.0	99.5	96.5	14
LMGEW//LN+LGXP	97.5	99.0	99.5	96.0	16

[a] Results extracted from original source.

amount of time between pictures taken. This database is organized into five sets of images: the gallery is Fa, and the test sets are Fb, Fc, Dup1, and Dup2. In the Fa set there are 1196 face images of different people. In the Fb set there are 1195 images of people with different gestures. Fc has 194 images with different illuminations. In Dup1 there are 722 images taken with between 0 and 34 months of difference from those taken for Fa. The Dup2 set has 234 images taken at least 18 months after the Fa set. The Fa set contains one image per person and is the Gallery set, while Fb, Fc, Dup1, and Dup2 are called test sets. Fig. 6 shows images from different sets of the FERET database: (a) a neutral image from the Fa set, (b) an image with a different expression from the Fb set, (c) an image with an illumination change from the Fc set, and (d) an image taken with several months difference from the Dup1 set.

The results obtained with LMGEW//LN-BTH and those published previously are presented in Table 2. The LMGEW//LN-BTH method obtained a total number of 79 errors with the FERET database. This result is better than all the best previously published results [33,35,36]. Even though LMGEW//LN-BTH has the best overall results, most of the improvement was produced in the Fb and Fc subsets. The total number of errors was reduced by 22.5% on images compared to the LMGEW//LN-BTH method. HEC [39] and LGBP+LGXP [40] obtained better results in the Dup2 subset, and LGBP+LGXP also obtained better results in subset Dup1. The LGBP+LGXP method reached 94% accuracy while LMGEW//LN-BTH obtained 92.66% in Dup1, and in Dup2 they reached 93% and 89.74%, respectively.

4. Results

4.1. Result comparison on LMGEW//LN-BTH

With the objective of comparing our results to those previously published, we summarized the best results using Gabor methods in face identification. Results of the literature review and proposed methods on face recognition are summarized in Tables 2–4 for different databases with frontal face cases. We also show results for faces with small pose variations; those that are rotated by ± 15 and ± 25° in the FERET database are shown in Table 5.

The first columns of each table show the face identification rates for different subsets of different databases. The last column in Tables 2, 3 and 5 shows the total number of errors on all subsets of the databases. For all the experiments the Borda count threshold (BTH) used is 0.85, obtained in our previous work [35].

4.1.1. LMGEW//LN-BTH Results using the FERET database
The FERET database is one of the most widely used benchmarks for face identification methods. To be able to compare our results to those of other methods, we followed the FERET face recognition protocol described in [41]. The FERET database has a large number of images with different gestures, illuminations, and a significant

4.1.2. LMGEW//LN-BTH Results using the AR face database
The AR database [45] contains frontal face images of men and women (60 females and 76 males) with different conditions of illumination, expression, and occlusion. Pictures were taken in two different sessions, with 13 pictures per session. We call Session 1, S1, and Session 2, S2. Seven of the 13 images contain illumination changes and gestures. In three images the person is wearing sunglasses, and in three other images, the person is wearing a scarf. As in [17] we
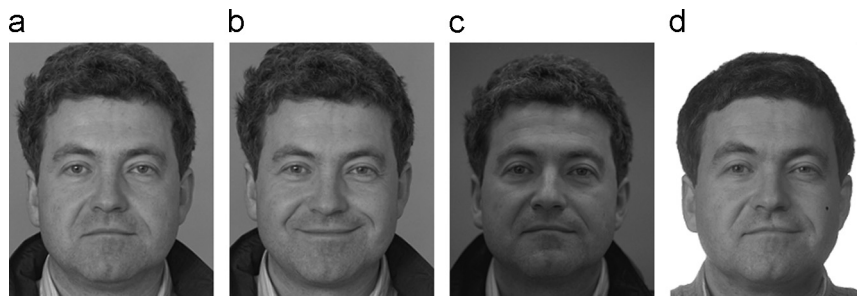
reaching the highest scores because each method solves different features better.

Fig. 6. FERET database examples. (a) Neutral image from set Fa, (b) expression image from set Fb, (c) illumination variation image from set Fc, and (d) time variation image from Dup1.
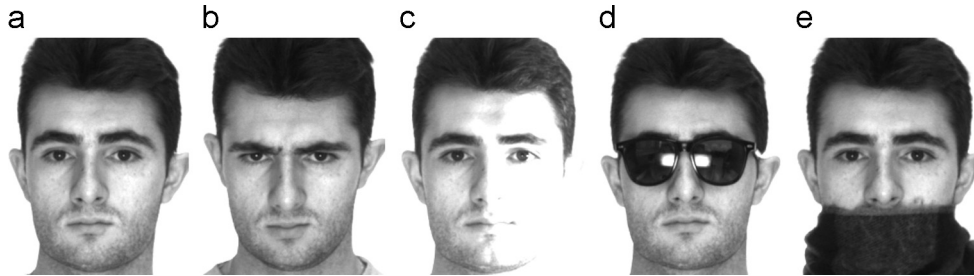

Fig. 7. AR database example images. (a) Neutral face image, (b) expression variation, (c) illumination variation, (d) face with sunglasses and (e) face with scarf.

randomly selected images of 50 men and 50 women which each had 26 images available.

Table 3 shows results for the LMGEW//LN-BTH and previously published methods in the AR database. We used a gallery set composed of seven images of Session 1 (neutral, expression, and illumination variation images), and five test subsets. Subset S2-Normal is similar to the gallery set, but contains images from Session 2. Subset Scarves contain faces occluded with Scarves for Sessions 1 and 2, and subset Sunglasses contains faces occluded with sunglasses. Fig. 7 shows images from the AR database: (a) a neutral face image, (b) an expression variation, (c) an illumination variation, (d) a face with sunglasses, and (e) a face with a scarf.

Results are almost the same as those of LMGEW-BTH, and better than the previously published identification methods. Only SRC has greater accuracy in the Sunglasses subset of AR, due to its robustness to occlusions.

4.1.3. LMGEW//LN-BTH Results using the FRGC 2.0 database

The FRGC 2.0 database [43] contains more than 50,000 images that are divided into training and testing partitions. The images are high resolution, with people looking frontally at the camera. There are images with and without controlled illumination.

The FRGC 2.0 database has a total of six experiments related to different subsets in the database [42,43]. Nevertheless, Experiments 1, 2, and 4 are the only ones for 2D face recognition; the rest of the experiments are for 3D face recognition. Experiment 1 contains controlled illumination images. Experiment 2 compares groups of images of the same individual, using the same images as in Experiment 1. Experiment 4 uses images under uncontrolled illumination, unfocussed images, and some with small pose variations. For each experiment, the Receiving Operator Characteristic (ROC) curves are constructed. ROC1 compares images taken within semesters, ROC2 within a year, and ROC3 during different semesters. Since our method was designed for the face identification problem, we adapted the original verification experiments of the FRGC 2.0 database to the identification problem using the Rank-1 method. We used images of Experiments 1 and 4 from the ROC3 partition. For Experiment 1, we used the same gallery set containing 7572 images and a sub-set of the test set without impostor

images with a total of 6512 images. For Experiment 4 the gallery set was formed with 7512 gallery images and 3256 test images. Fig. 8 shows examples of the FRGC 2.0 database; both (a) and (b) are gallery samples, (c) is a controlled image from Experiment 1, and (d) and (e) are uncontrolled images from Experiment 4.

Results of LMG methods are shown in Table 4. Experiment 1 shows a small difference between best and worst results, while our proposed method obtained the highest accuracy. In Experiment 4 the best score, 89.71%, was reached with the LMGEW-BTH, and the second best, 89.71%, was achieved using LMGEW//LN-BTH.

4.2. Entropy-like weighting on LGBP and LGXP features

We tested LGBP and LGXP computing entropy-like values for each local classifier, i.e., for each block. The feature vector of each block on the test image is compared with the same vector of the gallery image. Then, a comparison matrix is built containing comparisons between all blocks of each test image and the blocks of each gallery image. With this matrix, entropy-like values are computed and used to weight with the same strategy described in Section 3.1. The results for Fb, Fc, Dup1, and Dup2 are 99.16%, 97.94%, 86.29%, 79.06% using LGBP; and 97.66%, 95.88%, 79.64%, 76.50% using LGXP. Results showed small improvements (0.5% for LGBP, and 0.1% for LGXP) in face recognition when the entropy strategy was applied to LGBP and LGXP compared to the case where the entropy strategy was not applied. A possible explanation for these results is that the local features are already significantly reduced by the application of LDA over the histograms of LGBP and LGXP features. Therefore, the entropy strategy does not improve results in LGBP and LGXP as it does in the case of the LMG method where features are not reduced.

4.3. Results of the fusion of methods LMGEW//LN-BTH+LGBP and LMGEW//LN-BTH+LGXP

We also implemented the LGBP and LGXP methods proposed in [40], and combined them with LMGEW//LN-BTH to improve face identification rates in all subsets of the FERET and AR databases. We fused the methods LMGEW//LN-BTH+LGBP and LMGEW//LN-BTH+LGXP at the score level as shown in (7). S_1 denotes the
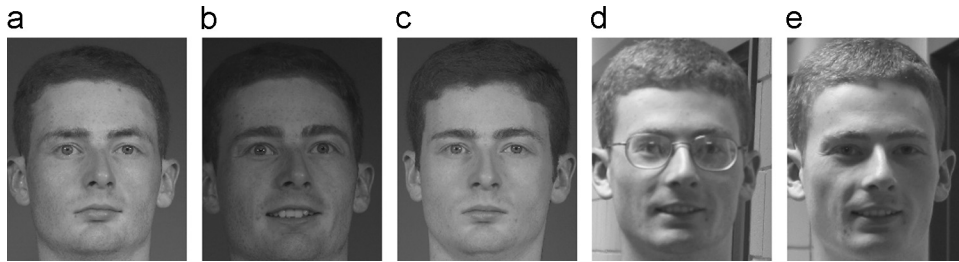
Fig. 8. Examples of face images from the FRGC2.0 database: (a) and (b) gallery images, (c) controlled images, (d) and (e) uncontrolled images.
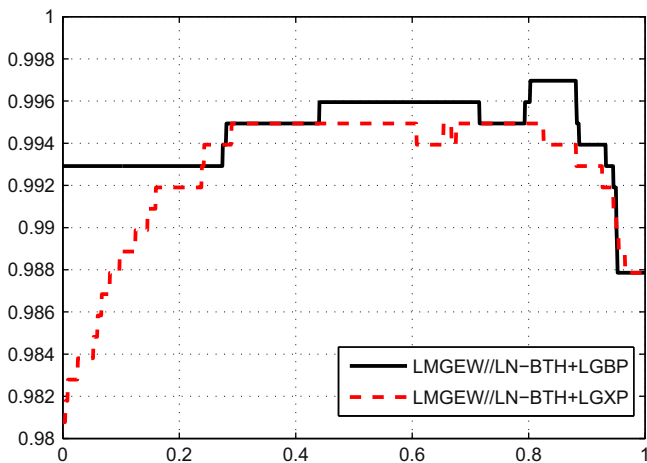

Fig. 9. Results for the fusion LMGEW//LN-BTH+LGBP and LMGEW//LN-BTH+LGXP as a function of the weight w in FERET database.

identification score of LMGEW//LN-BTH, S_2 the score of LGBP or LGXP.

Before fusing both methods, the ranges for the LMG, LGBP and LGXP scores were normalized to [0, 1]. LGBP and LGXP take values in the range $[-2, 16]$ while LMG takes values between $[100, 600]$. Therefore, the normalization was $S_{LGBP}^{norm} = (S_{LGBP} + 2)/18$, for LGBP and LGXP. For LMG the normalization was $S_{LMG}^{norm} = (S_{LMG} + 100)/500$. The weight w was varied from 0 to 1 as shown in Fig. 9. It can be observed that for values of w between 0.5 and 0.85 the fusion achieved the best results compared with any of the methods applied independently. We chose $w = 0.75$, and used this value for all the following experiments.

Fusion of the LMGEW//LN-BTH+LGBP and LMGEW//LN-BTH+ LGXP methods using the FERET database yielded the same results in Fb and Fc with 99.92% and 100% accuracy, respectively. Dup1 was improved by 1.57% and Dup2 by 0.59% compared with LGBP+LGXP. The total number of errors decreased from 77 in LGBP+LGXP to 48 in LMGEW//LN-BTH+LGBP which is a 38% improvement relative to previously published methods.

Fusion of LMGEW//LN-BTH+LGBP and LMGEW//LN-BTH+LGXP methods in the AR database also improved the best results obtained previously with LMG-based methods for all sub-sets. For the Normal S2 subset both fusions reached 100% accuracy, improving the 99.29% performance of LMGEW-BTH. In the Scarves subset both fusions improved compared with previous methods, and LMGEW// LN-BTH+LGBP reduced the error rate by 1%. In the Sunglasses subset, the fusion LMGEW//LN-BTH+LGXP method improved the results but could not reach the best results obtained by SRC [17].

4.4. Effect on face identification resulting from error in eye localization with the LMGEW//LN-BTH method

The LMG and derived methods require eye localization to align faces. Therefore, it is important to assess the effect of eye localization

error on face identification for the LMG method. We added noise in the eye coordinates for the LMGEW//LN-BTH method as was previously performed in [36]. The error distance radius varied between 1 and 10 pixels, and the angle between the center and the computed position between $0°$ and $360°$, both, radius and angle, using a uniform probability. Then, the images were aligned and cropped using the new eye coordinates. Fig. 10 shows the examples of alignment with noise in eye localization. Fig. 10(a) and (b) shows the difference between a well-aligned image and an image with 4 pixels of noise. Fig. 10(c) and (d) shows the difference between a well- aligned image and an image with 10 pixels of noise. Fig. 11 shows the face identification rate in the FERET database for subsets Fb, Fc, Dup1, and Dup2.

In the FERET database the image dimension is 256×384 pixels, and faces vary approximate between 75×95 to 180×260 pixels, which means that an error of 10 pixels in both eyes is significant. Results for the FERET subsets Fb and Fc (expression and illumination changes), show that face identification is almost unaffected by noise levels of up to 4 pixels. For errors greater than 4 pixels, the identification rate falls significantly with increasing eye localization error. For the Dup1 and Dup2 sets (time difference), the identification rate decreases significantly with more than 2 pixels of noise.

4.5. Results of face identification with pose variations

We tested the LMGEW//LN-BTH, LGBP, LGXP, and combined methods with the subsets bd, be, bf, and bg with pose variations of the FERET database as shown in Fig. 12. Table 5 shows the results of face recognition for small pose variations, and also the best previously published results.

Our proposed methods improve these results significantly for faces with small pose variations. LMGEW//LN-BTH showed a 46% in the error rate improvement compared to previous LMG-EJS-BIP-BTH results [35], reducing the total number of errors from 37 to 18. Results improved by 0.5% and 1.5% for $\pm 15°$ face pose rotation on the subsets be and bf, respectively. Results also improved 2.5% and 5% for subsets bd and bg, respectively, which have $\pm 25°$ face rotations. Fusion improved the results slightly, reducing the errors by 4 and 2 with LMGEW//LN+LGBP and LMGEW//LN+LGXP, respectively. These results show improvements in using LMGEW//LN-BTH and fusion with LGBP and LGXP for face identification with small pose variations.

5. Conclusions

In this work we proposed two new methods for face identification. The first one combines entropy-like weighted Gabor features with the local normalization of Gabor features. The second one fuses the entropy-like weighted Gabor features at the score level with the local Gabor binary pattern (LGBP) and the local Gabor XOR pattern (LGXP). We used the FERET, AR, and FRGC 2.0 databases to test and compare our results with those published previously.
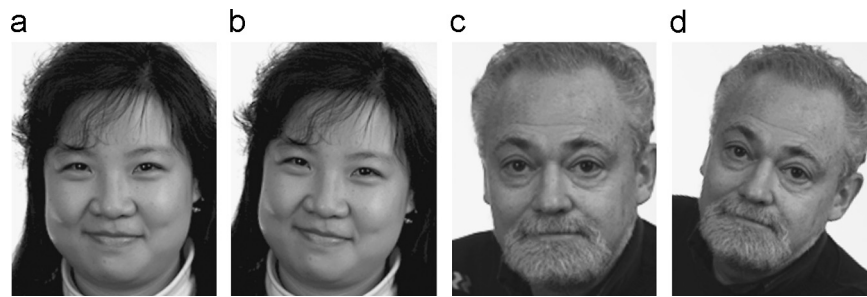
Fig. 10. Face images with gaussian noise in eye position. (a) Image aligned without noise, (b) the image aligned with noise of 4 pixels in both eyes, (c) another well aligned image, (d) image aligned with noise of 10 pixels.
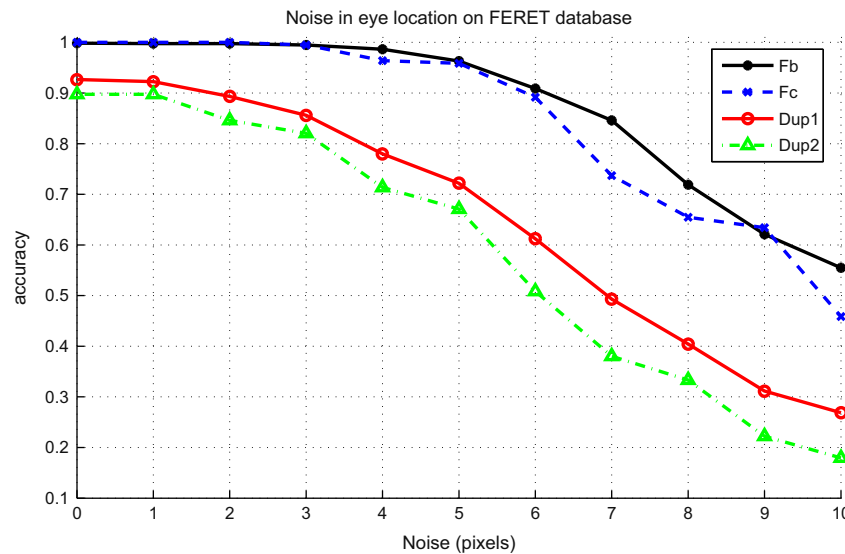

Fig. 11. Rank-1 face identification rate using the FERET database when noise between 1 and 10 pixels is added to the eye coordinates.
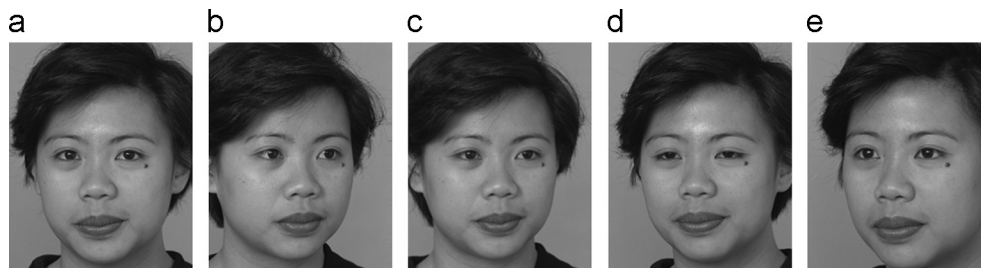

Fig. 12. FERET subsets with varying pose examples. (a) Frontal image, (b) $-25°$ pose, (c) $-15°$ pose, (d) $15°$ pose and (e) $25°$ pose.

LMGEW//LN-BTH showed good identification performance improving results of LMG and LMGEW. The method was assessed on different databases with varying illumination, small pose variations (up to $25°$), changing expressions, and using images taken on different dates and locations. Our proposed method shows robustness to illumination changes and gesticulations as shown in the results on the FERET, subsets Fb, Fc, the AR Normal subset and FRGC Exp. 1, with results over 99%. Robustness to illumination and spatial changes is due to the Gabor jets' capacity to deal with small spatial perturbations. The LN method, capable of eliminating the noise introduced by illumination changes, plays an important role as was shown in [37]. Improvements were found on the FERET subsets Dup1 and Dup2.

Results showed significant improvement relative to the LMG method with the application of LN and entropy-like weighting. LMG and LMGEW//LN-BTH can be compared viewing Tables 2 and 5, where results of frontal faces as well as faces with pose variation are shown. Improvements can be observed across all subsets of the FERET database, although they are most evident in Dup1 and Dup2. The error was reduced from 15% to 7.3% in Dup1 and from 20% to 10.3% in Dup2. This is a reduction of 52.3% in the error rate for Dup1 and 48.5% for Dup2. In addition, for pose variation of $25°$ the improvement in face recognition increased from 80.3% to 96.3%, i.e., a 16% increase. This improvement could be due to the entropy-like weights on the Gabor jets. The entropy-like function measures the consistency of each jet in one image compared to the same jet in the entire database. The weights are larger on face zones that are similar to each other on the frontal view of the face, while weights are smaller on other parts of the face.

LMGEW//LN-BTH, LGBP and LGXP individually have the highest scores on face identification on the databases used in this paper and we combined them. Results on fusion methods suggest that

different methods for face identification improve different features, and combining these features improves the overall results. Different methodologies applied to face recognition extract and emphasize different aspects of the face image and therefore, fusing them has a synergistic effect as shown in Fig. 9. In future work we will explore new methods for fusing extracted features such as SVMs, neural networks, and others.

Real face identification applications require automatic face detection and eye localization, which reduce performance in face recognition systems. We tested the effect of adding noise to the eye localization on face identification. We added noise from 1 to 10 pixels in each eye and the results indicate that up to 4 pixels of error do not have a significant effect on Fb and Fc subsets. In Dup1 and Dup2, the effect is significant with over 2 pixels of error in eye localization. Real-time eye localization systems [7] tolerate only less than 3 pixels of error.

As shown in this paper, fusion of entropy-like weighted phase and magnitude Gabor features, as well as local normalization, improved face identification significantly. In future work, exploring combinations with other types of features and the use of different fusion methods could be shown to improve current performance in face identification.

Conflict of interest statement

None declared.

Acknowledgments

References

[1] P.J. Phillips, H. Moon, S.A. Rizvi, P.J. Rauss, The FERET evaluation methodology for face-recognition algorithms, IEEE Transactions on Pattern Analysis and Machine Intelligence, 22 (10) (2000) 1090–1104, http://dx.doi.org/10.1109/34.879790.

[2] W. Zhao, R. Chellappa, P.J. Phillips, A. Rosenfeld, Face recognition: a literature survey, ACM Computing Surveys (CSUR) 35 (4) (2003) 399–458.

[3] R. Chellappa, J. Ni, V.M. Patel, Remote identification of faces: Problems, prospects, and progress, Pattern Recognition Letters 33 (14) (2011) 1849–1859. http://dx.doi.org/10.1016/j.patrec.2011.11.020.

[4] P. Campadelli, R. Lanzarotti, G. Lipori, Precise eye and mouth localization, International Journal of Pattern Recognition and Artificial Intelligence (IJPRAI) 23 (3) (2009) 359–377.

[5] C. Perez, V. Lazcano, P. Estévez, C. Held, Real-time template based face and iris detection on rotated faces, International Journal of Optomechatronics 3 (1) (2009) 54–67.

[6] C.A. Perez, V.A. Lazcano, P.A. Estevez, Real-time iris detection on coronal-axis-rotated faces, IEEE Transactions on Systems, Man, and Cybernetics, Part C: Applications and Reviews 37 (5) (2007) 971–978, http://dx.doi.org/10.1109/TSMCC.2007.900647.

[7] C. Perez, C. Aravena, J. Vallejos, P. Estévez, C. Held, Face and iris localization using templates designed by particle swarm optimization, Pattern Recognition Letters 31 (9) (2010) 857–868. http://dx.doi.org/10.1016/j.patrec.2009.12.029.27.

[8] C.A. Perez, C.A. Salinas, P.A. Estevez, P.M. Valenzuela, Genetic design of biologically inspired receptive fields for neural pattern recognition, IEEE Transactions on Systems, Man, and Cybernetics, Part B: Cybernetics 33 (2) (2003) 258–270, http://dx.doi.org/10.1109/TSMCB.2003.810441.

[9] C.A. Perez, G.D. Gonzalez, L.E. Medina, F.J. Galdames, Linear versus nonlinear neural modeling for 2-d pattern recognition, IEEE Transactions on Systems, Man and Cybernetics, Part A: Systems and Humans 35 (6) (2005) 955–964, http://dx.doi.org/10.1109/TSMCA.2005.851268.

[10] M.A. Turk, A.P. Pentland, Face recognition using eigenfaces, in: Proceedings of the CVPR '91. IEEE Computer Society Conference on Computer Vision and Pattern Recognition, 1991, pp. 586–591. http://dx.doi.org/10.1109/CVPR.1991.139758.

[11] P.N. Belhumeur, J.P. Hespanha, D.J. Kriegman, Eigenfaces vs. fisherfaces: recognition using class specific linear projection, IEEE Transactions on Pattern Analysis and Machine Intelligence 19 (7) (1997) 711–720, http://dx.doi.org/10.1109/34.598228.

[12] M.S. Bartlett, J.R. Movellan, T.J. Sejnowski, Face recognition by independent component analysis, IEEE Transactions on Neural Networks 13 (6) (2002) 1450–1464, http://dx.doi.org/10.1109/TNN.2002.804287.

[13] M. Sharkas, M.A. Elenien, Eigenfaces vs. fisherfaces vs. ica for face recognition; a comparative study, in: Ninth International Conference on Signal Processing, ICSP 2008, 2008, pp. 914–919.

[14] C. Podilchuk, X. Zhang, Face recognition using dct-based feature vectors, in: Proceedings of the IEEE International Conference on Acoustics, Speech, and Signal Processing ICASSP-96, vol. 4, 1996, pp. 2144–2147. http://dx.doi.org/10.1109/ICASSP.1996.545740.

[15] Z.M. Hafed, M.D. Levine, Face recognition using discrete cosine transform, International Journal of Computer Vision 43 (3) (2001) 167–188.

[16] M. Faundez-Zanuy, J. Roure, V. Espinosa-Duro, J.A. Ortega, An efficient face verification method in a transformed domain, Pattern Recognition Letters 28 (7) (2007) 854–858.

[17] J. Wright, A.Y. Yang, A. Ganesh, S.S. Sastry, Y. Ma, Robust face recognition via sparse representation, IEEE Transactions on Pattern Analysis and Machine Intelligence 31 (2) (2009) 210–227, http://dx.doi.org/10.1109/TPAMI.2008.79.

[18] A. Wagner, J. Wright, A. Ganesh, Z. Zhou, Y. Ma, Towards a practical face recognition system: robust registration and illumination by sparse representation, in: Proceedings of the IEEE Conference on Computer Vision and Pattern Recognition CVPR 2009, 2009, pp. 597–604. http://dx.doi.org/10.1109/CVPR.2009.5206654.

[19] R. Gross, I. Matthews, J.F. Cohn, T. Kanade, S. Baker, Multi-pie, Image and Vision Computing 28 (5) (2010) 807–813.

[20] R. He, W.-S. Zheng, B.-G. Hu, Maximum correntropy criterion for robust face recognition, IEEE Transactions on Pattern Analysis and Machine Intelligence 33 (8) (2011) 1561–1576, http://dx.doi.org/10.1109/TPAMI.2010.220.

[21] T. Ahonen, A. Hadid, M. Pietikainen, Face description with local binary patterns: application to face recognition, IEEE Transactions on Pattern Analysis and Machine Intelligence 28 (12) (2006) 2037–2041, http://dx.doi.org/10.1109/TPAMI.2006.244.

[22] F. Bianconi, A. Fernández, Evaluation of the effects of Gabor filter parameters on texture classification, Pattern Recognition 40 (2007) 3325–3335.

[23] D. Gabor, Theory of communication, Journal of Institute for Electrical Engineering 93 (III, 26) (1946) 429–457.

[24] V. Kyrki, J.-K. Kamarainen, H. Kälviäinen, Simple Gabor feature space for invariant object recognition, Pattern Recognition Letters 25 (2004) 311–318.

[25] M. Lades, J.C. Vorbruggen, J. Buhmann, J. Lange, C. von der Malsburg, R.P. Wurtz, W. Konen, Distortion invariant object recognition in the dynamic link architecture, IEEE Transactions on Computers 42 (3) (1993) 300–311, http://dx.doi.org/10.1109/12.210173.

[26] L. Wiskott, J.-M. Fellous, N. Kuiger, C. von der Malsburg, Face recognition by elastic bunch graph matching, IEEE Transactions on Pattern Analysis and Machine Intelligence 19 (7) (1997) 775–779, http://dx.doi.org/10.1109/34.598235.

[27] C. Liu, H. Wechsler, Gabor feature based classification using the enhanced fisher linear discriminant model for face recognition, IEEE Transactions on Image Processing 11 (4) (2002) 467–476, http://dx.doi.org/10.1109/TIP.2002.999679.

[28] W. Zhang, S. Shan, W. Gao, X. Chen, H. Zhang, Local Gabor binary pattern histogram sequence (lgbphs): a novel non-statistical model for face representation and recognition, in: Proceedings of the Tenth IEEE International Conference on Computer Vision ICCV 2005, vol. 1, 2005, pp. 786–791. http://dx.doi.org/10.1109/ICCV.2005.147.

[29] B. Zhang, S. Shan, X. Chen, W. Gao, Histogram of Gabor phase patterns: a novel object representation approach for face recognition, IEEE Transactions on Image Processing 16 (1) (2007) 57–68, http://dx.doi.org/10.1109/TIP.2006.884956.

[30] Z. Lei, S. Li, R. Chu, X. Zhu, Face recognition with local Gabor textons, in: Lecture Notes in Computer Science, Proceedings of the International Conference on Advances in Biometrics, Seoul, Korea, vol. 4642, 2007, pp. 49–57.

[31] S. Xie, S. Shan, X. Chen, X. Meng, W. Gao, Learned local Gabor patterns for face representation and recognition, Signal Processing 89 (2009) 2333–2344.

[32] H.V. Nguyen, L. Bai, L. Shen, Local Gabor binary pattern whitened pca: a novel approach for face recognition from single image per person, in: Proceedings of the Third International Conference on Advances in Biometrics, Alghero, Italy, Lecture Notes in Computer Science, vol. 5558, 2009, pp. 269–278.

[33] J. Zou, Q. Ji, G. Nagy, A comparative study of local matching approach for face recognition, IEEE Transactions on Image Processing 16 (10) (2007) 2617–2628, http://dx.doi.org/10.1109/TIP.2007.904421.

[34] T.K. Ho, J.J. Hull, S.N. Srihari, Decision combination in multiple classifier systems, IEEE Transactions on Pattern Analysis and Machine Intelligence 16 (1) (1994) 66–75, http://dx.doi.org/10.1109/34.273716.

[35] C.A. Perez, L.A. Cament, L.E. Castillo, Methodological improvement on local Gabor face recognition based on feature selection and enhanced Borda count, Pattern Recognition 44 (2011) 951–963.

[36] C.A. Perez, L.A. Cament, L.E. Castillo, Local matching Gabor entropy weighted face recognition, in: Proceedings of the IEEE Int Automatic Face & Gesture Recognition and Workshops (FG 2011) Conference, 2011, pp. 179–184. http://dx.doi.org/10.1109/FG.2011.5771394.

[37] C.A. Perez, L.E. Castillo, L.A. Cament, Illumination compensation method for local matching Gabor face classifier, in: Proceedings of the International

Conference on Optomechatronic Technologies (ISOT) Symposium, 2010, pp. 1–5. http://dx.doi.org/10.1109/ISOT.2010.5687330.

[38] A. Franco, D. Maio, D. Maltoni, 2d face recognition based on supervised subspace learning from 3d models, Pattern Recognition 41 (12) (2008) 3822–3833.

[39] Y. Su, S. Shan, X. Chen, W. Gao, Hierarchical ensemble of global and local classifiers for face recognition, IEEE Transactions on Image Processing 18 (8) (2009) 1885–1896, http://dx.doi.org/10.1109/TIP.2009.2021737.

[40] S. Xie, S. Shan, X. Chen, J. Chen, Fusing local patterns of Gabor magnitude and phase for face recognition, IEEE Transactions on Image Processing 19 (5) (2010) 1349–1361, http://dx.doi.org/10.1109/TIP.2010.2041397.

[41] P.J. Phillips, H. Wechsler, J. Huang, P. Rauss, The feret database and evaluation procedure for face recognition algorithms, Image and Vision Computing 16 (5) (1998) 295–306.

[42] P.J. Phillips, P.J. Flynn, T. Scruggs, K.W. Bowyer, J. Chang, K. Hoffman, J. Marques, J. Min, W. Worek, Overview of the face recognition grand challenge, in: Proceedings of the IEEE Computer Society Conference on Computer Vision and Pattern Recognition CVPR 2005, vol. 1, 2005, pp. 947–954. http://dx.doi.org/10.1109/CVPR.2005.268.

[43] P.J. Phillips, P.J. Flynn, T. Scruggs, K.W. Bowyer, W. Worek, Preliminary face recognition grand challenge results, in: Proceedings of the Seventh International Conference on Automatic Face and Gesture Recognition FGR 2006, 2006, pp. 15–24. http://dx.doi.org/10.1109/FGR.2006.87.

[44] J. Kittler, M. Hatef, R.P.W. Duin, J. Matas, On combining classifiers, IEEE Transactions on Pattern Analysis and Machine Intelligence 20 (3) (1998) 226–239, http://dx.doi.org/10.1109/34.667881.

[45] A. Martinez, R. Benavente, The ar face database, CVC Technical Report 24.

Leonardo A. Cament received the BS and PE in Electrical Engineering from Universidad de Chile in March 2008 with the highest honors. He is a PhD candidate at the Department of Electrical Engineering, Universidad de Chile. His main interests in research are pattern recognition applied to eye detection, face recognition and human machine interfaces.

Luis E. Castillo received the BS and PE in Electrical Engineering from Universidad de Chile in December 2008. He is a PhD candidate at the Department of Electrical Engineering, Universidad de Chile. His main interests are pattern recognition applied to face recognition and illumination compensation.

Juan P. Perez received the BS in Electrical Engineering from Universidad de Chile in December 2012. He is a PhD candidate at the Department of Electrical Engineering, Universidad de Chile. His main interests are pattern recognition applied to face recognition and clustering algorithms.

Francisco J. Galdames received the BS and PE in Electrical Engineering and the MS degree in Biomedical Engineering all from Universidad de Chile in 2006. In 2012 he obtained the PhD from Universidad de Chile and Université Joseph Fourier. He is postdoctoral fellow at Universidad de Chile. His interests include pattern recognition applied to face recognition and 3D modeling.

Claudio A. Perez received the BS and PE in electríical engineering and the MS degree in biomedical engineering all from Universidad de Chile in 1980 and 1985, respectively. He was a fulbright student at the Ohio State University where he obtained the PhD in 1991. In 1990 he was a presidential fellow and received a Graduate Student Alumni Research Award from O.S.U. In 1991 he received a fellowship for Chilean scientists from Fundacion Andes. He was a visiting scholar at UC, Berkeley in 2002 through the Alumni Initiatives Award Program from Fulbright Foundation. Currently he is a professor at the Department of Electrical Engineering, University of Chile, where he was the chairman from 2003 to 2006. His research interests include face and iris biometrics, pattern recognition and human–machine interfaces. He is member of the editorial board of the International Journal of Optomechatronics and BMC Neuroscience and a Senior Member of the IEEE-SMC and IEEE-CIS, member of Sigma-Xi and OSU Alumni Association.